Sustainable Structures
ISSN: 2789-3111 (Print); ISSN: 2789-312X (Online)
http://www.sustain-dpl.com/journal/sust
DOI: 10.54113/j.sust.2024.000041

ORIGINAL ARTICLE

Experimental, theoretical and numerical study on the shear stress of adhesive layer in FRP-bamboo scrimber composite beams

Yongchao Zhang[a], Man Liu[a], Caimei Liu[a], Xizhi Wu[a,b,*], Yutong Li[a], Xianjun Li [a], Zhangjing Chen[c *]

[a] College of Materials Science and Engineering, Central South University of Forestry and Technology, Changsha,410082, China.
[b] Guangzhou Tech-long Packaging Machinery Co., Ltd. Guangzhou, 510000, China.
[c] Department of Sustainable Biomaterials, Virginia Tech University, Blacksburg VA24061, USA
*Corresponding author: Xizhi Wu, E-mail: wuxizhi2006@126.com.

Abstract: The adhesive layer is an important factor affecting the mechanical properties of FRP- bamboo scrimber composite beams (FBSCB). However, studies on the interfacial shear stresses in the adhesive layers with both ends of FRP and bamboo scrimber beam aligned have been rarely reported. To this end, a two-parameter theoretical calculation model and a finite element model (FEM) based on cohesive zone model were hereby established to solve for the adhesive layer interface shear stresses, which was verified by four-point bending experiments. The results show that both the two-parameter theoretical model and the FEM can effectively compute the shear stress of the adhesive layer. Meanwhile, the FEM simulation results not only reflect the detailed changes of the shear stress, but also provide a better analysis of the shear stress at the adhesive layer with a small fluctuation range. There are three zones of shear stress at the adhesive layer of FBSCB under four-point bending load, i.e., the bending and shearing zone, the transition zone and the pure bending zone. In the bending and shearing zone, the shear stress of the adhesive layer interface increases 2.61 times and 2.5 times, respectively when the thickness and elastic modulus of FRP increase three times. However, the stress remains constant at zero in the pure bending zone.

Keywords: Bamboo scrimber; FRP; adhesive layer; interface stresses; cohesive zone model

1 Introduction

With the growing interest in green buildings and environmentally friendly materials, a significant increase in research on natural materials such as bamboo, wood and straw has been experienced by scholars. Bamboo has received much attention as a natural biomass composite material that can be regenerated after being cut and can be degraded after being discarded, which has a short growth cycle as well [1-3]. However, the use of natural bamboo as a construction material is limited by the small diameter of the culm, the thin wall and hollow center, and easiness to crack. Overcoming the above limitations of natural bamboo, bamboo scrimber is a new type of bamboo-based composite material made of bamboo bundles or fibrillated bamboo veneer as a component unit, which is pressed by smooth-grained grouping, hot or cold pressing and gluing. Bamboo scrimber has been extensively used in indoor flooring, furniture manufacturing, decoration, outdoor flooring, building structural elements, wind turbine blades, etc. [4]. However, as a flexural member, the bamboo scrimber beam is subject to the

Received: 24 October 2023; Received in revised form: 6 May 2024; Accepted: 18 May 2024

disadvantages of low cross-sectional stiffness, high bending deflection and limited span capacity, failing to meet the requirements of large span structures [5, 6]. In order to eliminate these shortcomings, fiber reinforced polymer (FRP) [7, 8], anchored structures [9], and internally embedded reinforcement materials [10] were proposed for the reinforcement of bamboo scrimber beams. On the one hand, FRP materials are provided with high strength, light weight and good corrosion resistance, while on the other, a large number of experiments have proved that FRP materials can improve the flexural stiffness and load-bearing capacity of beams [11-15]. Therefore, FRP materials are widely used as reinforcement materials for bamboo scrimber beams.

In composite beams containing an adhesive layer, the stress distribution of the adhesive layer has an important influence on the failure model and the location of damage of the composite beam, making it necessary to get a better understanding of the stress distributions of the bonding interface. For this purpose, the adhesive layer interface of composite beams has been extensively studied. Goland [16] proposed a two-parameter model (G-R model) assuming shear and normal stresses in the adhesive joint, which were invariant along the thickness direction, forging the foundation for the study of stresses at the adhesive interface. Smith [17] derived the closed numerical solution based on the G-R model by assuming the reinforced beam, reinforcing the material as Euler-Bernoulli beams and neglecting the effect of shear deflection.

However, in the case of the thicker adhesive layer, there are differences in the stress distribution between the two interfaces above and below the adhesive layer, and the two-parameter model cannot obtain accurate results. Therefore, on the basis of the two-parameter model, Wang [18] assumed that the positive stresses on the upper and lower sides of the adhesive layer were different and took the deflection of the adhesive layer as the third parameter to propose a three-parameter model, providing a new idea to solve the adhesive layer interface stresses for thicker adhesive layers. Chen [19] introduced the longitudinal and transverse displacements of the adhesive layer as independent new parameters and proposed a four-parameter model. However, the transverse displacement was assumed to be invariant across the thickness, and the shear deformation and bending moment of the adhesive layer were neglected, but the solution process was extremely complicated. Based on Chen's four-parameter model, Du [20] proposed an improved model to obtain a closed stress solution. The internal forces of the adhesive layer were assumed to comply with the Timoshenko beam theory, so that the shear deformation and bending moment of the adhesive layer could be considered, and the correctness of the theoretical model was verified by finite element simulation.

In general, although the three-parameter and four-parameter models can calculate the adhesive layer stresses along the thickness direction for more accurate solutions, the assumption for the adhesive layer thickness, which usually exceeds 2 mm, is still far beyond the thickness of the adhesive layer in FRP-reinforced bamboo scrimber beams. Meanwhile, the stresses on the upper and lower surfaces of the adhesive layer differ only within 5 mm from the end, and are basically the same after exceeding 5 mm, but the complexity of the calculation cannot be compared with the more parameters introduced.

Wu [21] established a finite element model of carbon fiber reinforced polymer (CFRP)-reinforced steel plates based on the cohesion zone model (CZM), which was tested by experiments to reveal the peeling mechanism of the adhesive layer.

Herein, inspired by the method of mutual verification through theoretical, experimental and finite element simulation, corresponding simulations were used to investigate the FBSCB shear stress of the adhesive layer. Firstly, three groups of four-point bending experiments were carried out on the composite beam, and the average interfacial shear stress was obtained by applying strain gauges to the FRP surface. Secondly, considering the thin thickness of the adhesive layer in the experiments (all less than 1mm), a two-parameter model was adopted to develop the theoretical formula for the shear stress of the adhesive layer, and then a FEM of the composite beam was established based on CZM. Finally, the theoretical model and FEM were proved by experimental data. The influence of FRP thickness and types to shear stress of the adhesive layer was discussed. Overall, the research results refine the theory of stress of the adhesive layer of bamboo scrimber composite beams.

2 Experimental Tests

2.1 Materials

2.2.1 Bamboo scrimber

Herein, the bamboo scrimber involved was manufactured by Wuxi Bodai Bamboo Wood Industry Co. Ltd., made from Moso bamboo, and was mechanically milled, dried, dipped and dried again in turn to produce oriented bamboo bundles along the grain direction. The Moso bamboo (*Phyllostachys pubescens*), aged 3-5 years, was harvested from Jiangxi Province in the south part of China. Moso bamboo culms were processed into interconnected and longitudinally continuous bamboo fibers by flattening, defibring and caramelizing. The bamboo bundles were produced in the form of single bundles, with a length of 2.2 m and a thickness of 5-7 mm. The drying process was carried out at a temperature of 50 ℃ for 8 h, after which, the moisture content was around 11%. The prepreg adhesive was water soluble phenolic resin adhesive from Guangdong Taier Co., Ltd., with 45% solid content and 8 minutes of immersion time. In order to reduce the variation in material properties caused by external factors, the same batch of raw materials was hereby chosen.

To obtain the longitudinal modulus of elasticity, tensile strength and compression strength of bamboo scrimber, uniaxial tensile and compression tests were performed, referring to ASTM D143-09 [22] and ASTM D695-02a [23] experimental standard methods, with a number of 5 specimens involved, respectively. The dimensions of parallel-grained tension specimens are shown in **Fig. 1**, with the effective middle dimension of 63 mm×10 mm. The dimensions of the compression specimen are 50 mm×50 mm×150 mm, where the length parallel to the grain is 460 mm.

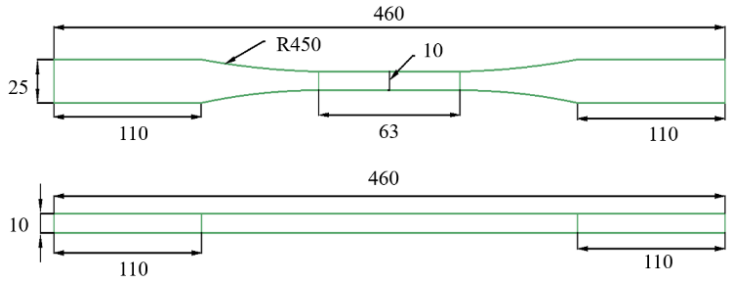

Fig. 1. Dimensions of bamboo scrimber tension specimens (units: mm).

The stress-strain curve of bamboo scrimber is shown in **Fig. 2**. In tension, the relationship between axial stress and axial strain is linear. The compressive stress-strain curve is non-linear and can be divided into three stages: the first is the elastic stage (0~27 MPa), in which the stress-strain curve increases linearly until the elastic limit stress of 27 MPa, represented by Point A; the second is an elastoplastic stage (27~80 MPa), in which the growth rate of axial stress decreases with increasing strain when the stress exceeds the elastic limit, represented by Point B and the stress-strain curve shows a non-linear relationship; and the third is the post-yield stage(80~82.67MPa), in which the axial strain continues rapidly to increase and the stress slowly rises or almost maintains constant. The stress-strain curve presents a flat linear relationship.

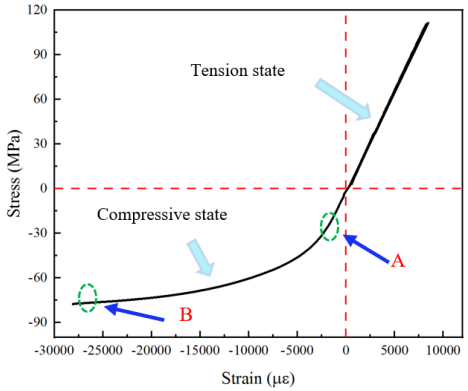

Fig. 2. Stress-strain relationships of bamboo scrimber.

The mechanical properties of the bamboo scrimber measured are shown in **Table 1**. The average

values of ultimate tensile strength, ultimate tensile strain and Young's modulus in tension are 109.52 MPa, 0.0071 and 12.71 GPa, respectively, while the ultimate compression strength, strain and elastic modulus of the bamboo scrimber are 82.67 MPa, 0.034 and 12.83 GPa, respectively. The numerical of the elastic modulus in tension and in compression are very close to each other, and 12.71 MPa was thus used uniformly for further analysis.

Table 1. Mechanical properties of bamboo scrimber

Property	Average value	Coefficient of variation
Ultimate tensile strain	0.0071	1.69%
Ultimate tensile strength, MPa	109.52	13.28%
Young's modulus in tension, GPa	12.71	2.91%
Ultimate compression strain	0.034	0.58%
Ultimate compression strength, MPa	82.67	6.02%
Young's modulus in compression, GPa	12.83	11.69%

2.1.2 FRP

Two FRP materials, i.e., Carbon Fiber Reinforced plastic (CFRP) and Glass Fiber Reinforced plastic (GFRP), were hereby selected. The fabrication and tension test of FRP was conducted with reference to GB/T 3354-1999 [24]. The dimensions of the specimens are shown in **Fig. 3**, five of each specimen. The measured thickness of CFRP is 0.21 mm and 0.25 mm for GFRP. The experimental apparatus is an American MTS electro-hydraulic servo universal material testing machine, MTS810, with a maximum axial load capacity of 100 kN, with hydraulic pressure used for driving and a loading rate of 0.5 mm/min adopted.

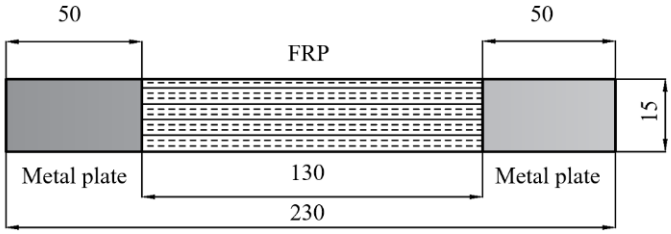

Fig. 3. Dimensions of FRP tension specimens (units: mm).

The average mechanical properties of CFRP and GFRP are listed in **Table 2**. The stress-strain relationship of FRP composite material in tension is linear until failure, and the mean values of ultimate tensile strength, ultimate tensile strain and tensile modulus of elasticity for CFRP are 728.76 MPa, 0.0098 and 90.1 GPa, respectively. The ultimate tensile strength, ultimate tensile strain and tensile modulus of elasticity of GFRP have average values of 372.8 MPa, 0.012 and 31.2 GPa, respectively. In contrast, the tensile modulus of elasticity and tensile strength of CFRP are greater than those of GFRP.

Table 2. Average experimental mechanical properties in tension of FRP

Specimen	Property	Average value	Coefficient of variation
CFRP	Young's modulus, GPa	90.1	8.65%
	Ultimate tensile strength, MPa	774.98	8.45%
	Ultimate tensile strain	0.0098	8.87%
GFRP	Young's modulus, GPa	31.2	2.31%
	Ultimate tensile strength, MPa	372.77	5.29%
	Ultimate tensile strain	0.012	5.00%

2.2 Specimen preparation

The bamboo scrimber beams were ordered from the factory. According to ASTM D198-02[25] experimental method for timber frame beams, the test piece was determined to be rectangular in cross section, with dimensions L×W×H of 1932 mm×70 mm×106 mm and length in the direction of the bamboo bundle with the grain.

Fig. 4 depicts the process of making FBSCB: firstly, before applying glue, the adhesive surface of the bamboo scrimber beams was polished and cleaned, and processed with alcohol to remove impurities

and dust; secondly, the epoxy resin adhesive was evenly applied to the surface of the bamboo scrimber beams, the cut FRP cloth was laid from one side, and appropriate pressure was exerted with a rubber plate to squeeze out the air bubbles and extra glue and ensure the uniformity of the adhesive layer. The epoxy bonding agent Sikadur-330 was used in this paper, the mechanical properties of which had been clarified by the manufacturer in advance [21]; Next, cling film was placed on the FRP to prevent the adhesive from bonding to the upper body, a smooth plate larger than the surface area of the beam was placed on the cling film, and 50kg weights were placed uniformly on the sheet and waited for 1 to 2 h; Finally, the adhesive layer was removed, pressed evenly with a load of about 1 ton and statically stressed at room temperature for 7 to 10 days when not fully cured. According to previous experience, the adhesive performance was better when the curing pressure of FBSCB was about 0.1 MPa. The practical dimensions of the composite beam are listed in **Table 3** below. Herein, the thickness of the adhesive layer was determined by that of the bamboo scrimber beams after bonding FRP and subtracting the thickness of the unreinforced bamboo scrimber beams, which might lead to uneven thickness of the adhesive layer for different specimen.

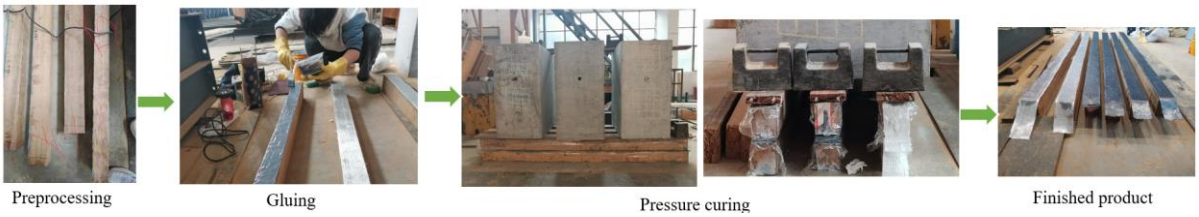

Fig. 4. Process of making FRP- bamboo scrimber composite beams

Table 3. Practical parameters of composite beam specimens

Group	Specimen	Actual dimensions (mm)	FRP types	Weight of bamboo scrimber beam (kg)	Thickness of adhesive layer (mm)
1	CB1-A	1932×106.68×71.03	CFRP	16.6	0.34
	CB1-B	1932×107.30×71.23	CFRP	16.6	0.38
2	CB3-A	1932×107.65×71.23	CFRP	16.5	0.36
	CB3-B	1932×107.64×70.18	CFRP	16.6	0.36
3	GB1-A	1932×106.76×71.77	GFRP	17	0.34
	GB1-B	1932×107.78×70.50	GFRP	16.5	0.52

(The first letter of the specimen numbers indicates the FRP types, the second letter indicates the bamboo scrimber, the number denotes the FRP layers and the third letter indicates the repeated sample code.)

2.3 Flexural test setup and procedure

The experimental loading device is shown in **Fig. 5**. Herein, both supports were placed symmetrically and horizontally along the central axis in the length and width direction, and the actual distance between the pressed areas was 1,700 mm. The hydraulic jack load was uniformly imposed by the pressure transducer through the distribution beam onto the two loading points. The hydraulic jack had a maximum axial load carrying capacity of 100 kN and a pressure transducer range of 100 kN. A laser displacement sensor (LD) was arranged directly below the span to measure the deflection, and the LD was a Panasonic HG-C1030 with a range of 160 mm and an accuracy of 0.2 mm.

The detailed locations of the strain gauges are shown in **Fig. 5**, distributed on the axis of the lower surface of the FRP plate, all in the left half of the center of symmetry of the composite beam. They were primarily used to monitor the FRP stresses at the purely bending part, the bending and shearing section and the loading point of the beam. The strain gauges were BE120-3AA from AVIC Electro-Mechanical Instruments Co., Ltd. The strain gauges had a sensitive grid length of 3 mm and a 120 Ω standard electrical resistance, and DHDAS from Donghua Co., Ltd. was used for the data collection.

The experiments were carried out using manual hydraulic cylinder loading. The test piece was first preloaded to keep the loading rate steady and uniform, after loading it to 5 kN and maintaining it for 3 minutes and then removing it. The experiment was repeated twice to confirm that the experimental setup was working properly and to eliminate the space between the loading device and the specimen. For formal loading, when the load was less than 20 kN, the hand cylinder was continuously and slowly

loaded, one level was loaded at 2 kN intervals after 1 minute of stability, the displacement, load, strain and other data were then recorded; when the load was greater than 20kN, it was reduced to one level at 1 kN apart, the stabilization time rose to 2 minutes, and the relative data were recorded until the specimen was damaged. During the experiment, the damage of the specimen was observed at all times, while photos and videos were taken. Finally, the ultimate loads of the specimens and their damage patterns were recorded.

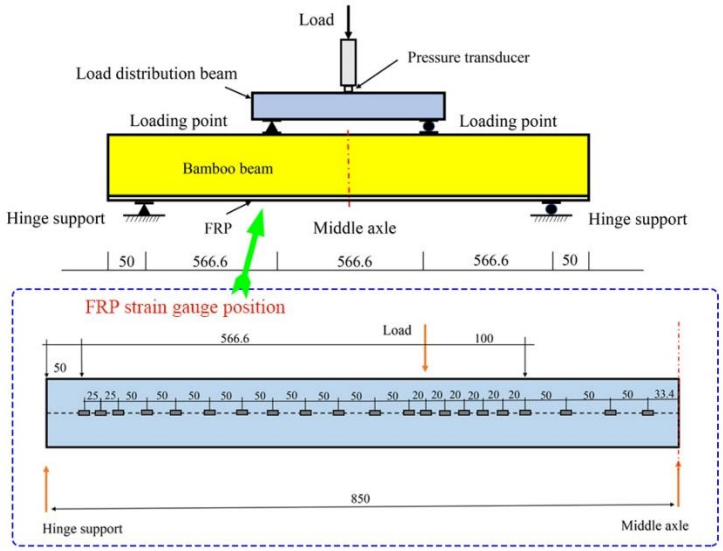

Fig. 5. Test setup for four-point bending test and configurations of strain gauges (units: mm).

3 Experimental Results

3.1 Failure mode

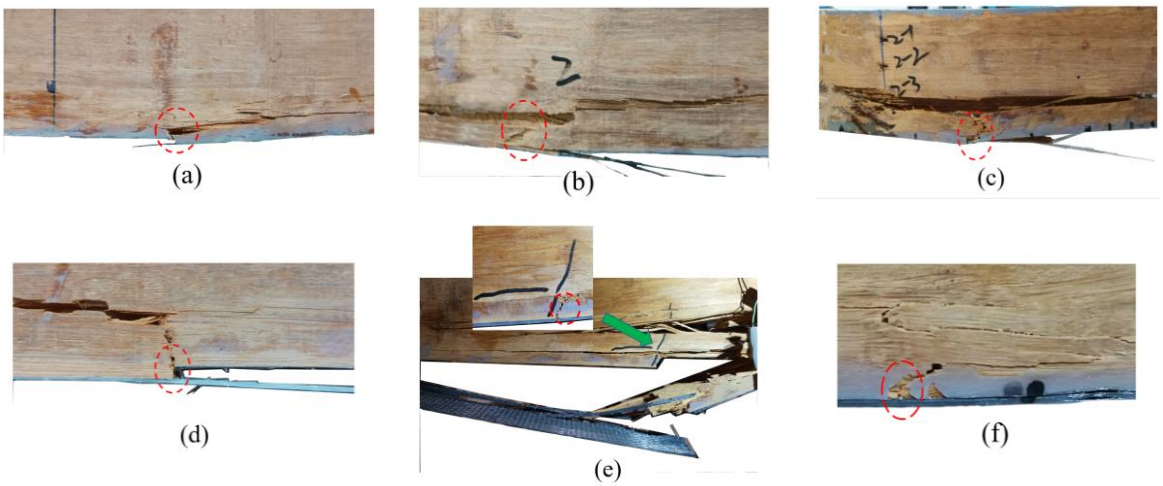

Fig. 6. Part of the FBSCB failure model: (a) CB1-A; (b) CB1-B; (c) GB1-A; (d) GB1-B; (e) CB3-A; and (f) CB3-B.

The failure of FBSCB is illustrated in **Fig. 6**. There were two failure modes: failure mode 1 was the simultaneous fracture of the bamboo scrimber beams and the FRP material, as in specimen GB1-A. The specimen had no fracture sound at the beginning of the experiment, and when the applied load reached 54 kN, the GFRP and the bamboo scrimber beam broke at the same time and the load dropped rapidly, which ended the experiment. Failure mode 2 was that the bamboo scrimber beams were the first to break down, causing the FRP to drop off from the bottom of the composite beams and the failure of the whole specimen, as in specimen CB1-A. When the imposed load was 58.2 kN, the first break of the bamboo filaments was heard and no cracks were visible on the surface. Small cracks appeared at the bottom of the side of the composite beam when the applied load was 61 kN, resulting in delamination

of the bamboo fibers and extending to the sides until damage. Specimens CB1-B, CB3-A, CB3-B and GB1-B also belonged to failure model 2. The loads of the initial bamboo wire fracture noise were 60 kN, 64 kN, 72 kN and 60 kN, respectively.

3.2 Load-displacement curves

Fig. 7(a) shows load-displacement curves of FBSCB. It is apparent that the load-displacement curves for all specimens can be divided into three stages, i.e., the initial linear-elastic stage, the nonlinear stage and the abrupt breaking stage. The load increases almost linearly with displacement at the initial linear elastic stages. Then, the specimen load-displacement curves distort nonlinearly due to plastic deformation generated by the bamboo scrimber beam in the top compression zone, which results in slowly decreasing cross sectional stiffness with an increasing load. Finally, considering the fragile fracture in the tension area at the bottom of the specimen, accompanied by a loud crash, the nonlinear phase ends and enters the stage of abrupt failure. It can be obtained that the composite beam stiffness of 3 layer CFRP is 1.14 times of 1-layer in the presence of the same cross-sectional conditions.

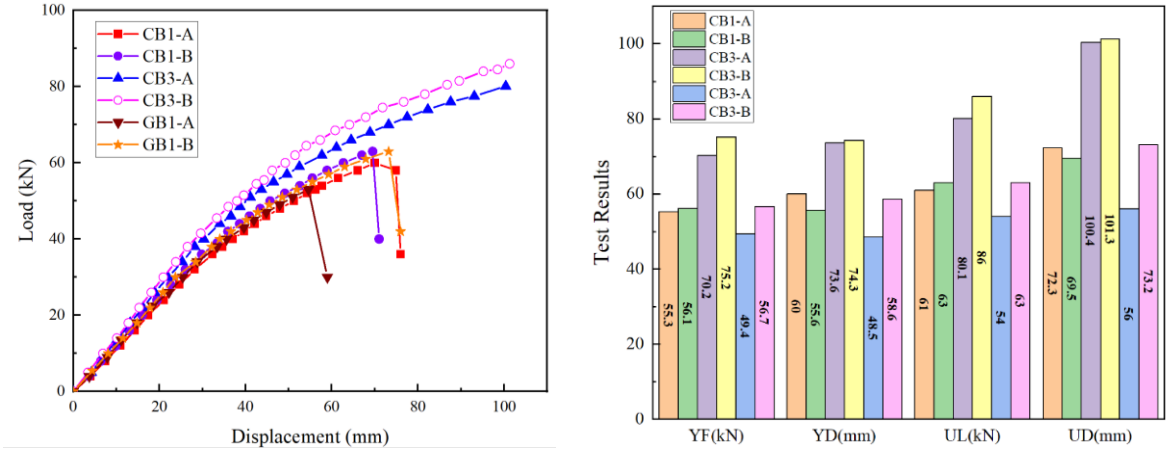

(a) (b)

Fig. 7. (a) Load–displacement curves of the FBSCB; (b) Test results of all composite beam specimens. (YF indicates the Yield force; YD, the Yield displacement; UL, the Ultimate load; UD, the Ultimate displacement).

Table 4. Average of test results of all composite beam specimens

Group	YF(kN)	YD(mm)	UL(kN)	UL(kN)
1	55.7	57.8	62	70.9
2	72.7	73.95	83.05	100.85
3	53.05	53.55	58.5	64.4

The yield displacements and yield loads were often decided through geometric mapping, the R. Park method and the equivalent elastoplastic energy method for load-displacement curves with no obvious yield point. The equivalent elastoplastic energy method [26] was based on the principle of energy equivalence to transform the actual skeleton curve into an ideal elastoplastic curve. The method had explicit physical significance and was hereby used to work out yield displacements and yield loads. The mechanical properties of the FBSCB are shown in **Fig. 7**(b) and **Table. 4**. The average yield load, average yield displacement, average ultimate load and average ultimate displacement of the specimens in Group 2 are 30.5%, 27.9%, 33.9% and 42.2% greater than those in Group 1, respectively. Thus, not only the yield load and ultimate load of the composite beam with three-layer CFRP is larger than that of the composite beam with one-layer CFRP, but also its yield displacement and ultimate displacement present the same phenomenon. A gradual downward shift is observed in the center line of the composite beam as the number of CFRP layers increases, reducing the tensile force on the bottom bamboo scrimber.

3.3 Stresses in the adhesive layer

The forces of the adhesive layer are shown in **Fig. 8**. The theoretical calculations are based on the following assumptions:

(1) The internal stresses of the adhesive layer are assumed to be constant in the direction of its thickness;

(2) All layers and bonding layers are isotropic, homogeneous linear elastic materials with no sliding at all adhesive interfaces;

(3) The internal forces of the adhesive layer, FRP reinforcement and bamboo scrimber beam conform to Euler-Bernoulli beam theory;

(4) The tensile stresses of the bamboo scrimber beam and the FRP reinforcement are uniformly distributed over the width of their cross-section.

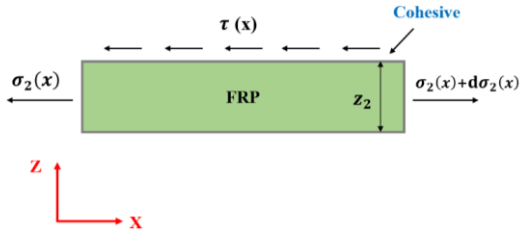

Fig. 8. Stress of the adhesive layer.

The FRP plate has width b_1, height z_2, positive stress $\sigma_2(x)$, and shear stress of the adhesive layer $\tau(x)$. The equilibrium equation is thus established along the x-direction as follows:

$$b_2 z_2 (\sigma_2 + d\sigma_2) = b_2 z_2 \sigma_2 + \tau b_2 dx \tag{1}$$

The simplification of Eq. (1) gives:

$$\tau = z_2 \frac{d\sigma_2}{dx} \tag{2}$$

The constitutive equation for FRP is given as follows:

$$\sigma_2 = \varepsilon_2 E_2 \tag{3}$$

Substituting Eq. (3) into (2) yields the differential equation for the interfacial stress in the adhesive layer as follows:

$$\tau = z_2 E_2 \frac{d\varepsilon_2}{dx} \tag{4}$$

Substituting the strain $\varepsilon_{2,i}$ of the FRP plate at each point measured by the strain gauges into Eq. (4), the interfacial shear stress of the adhesive layer at every measured point can be found as:

$$\tau_i = z_2 E_2 \frac{\varepsilon_{2,i+1} - \varepsilon_{2,i}}{\Delta_{i,i+1}} \tag{5}$$

In Eq.5 above, $\Delta_{i,i+1}$ is the spacing between the ith and i+1st strain gauges, with the initial value of i being 1 and the maximum limit being n. The spacing remains consistent with the previous section. The shear stress is the average interfacial shear stress between two adjacent strain gauges, the value of which is related to the thickness of the FRP sheet and the spacing between the gauges.

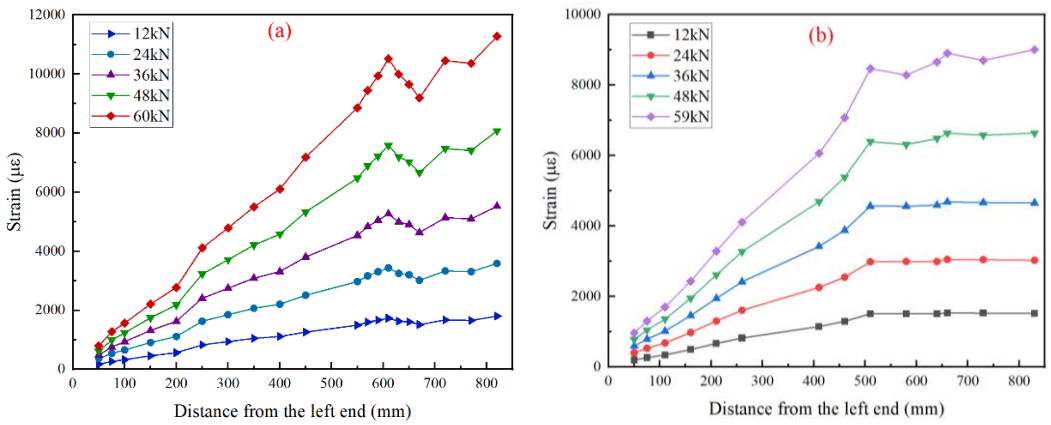

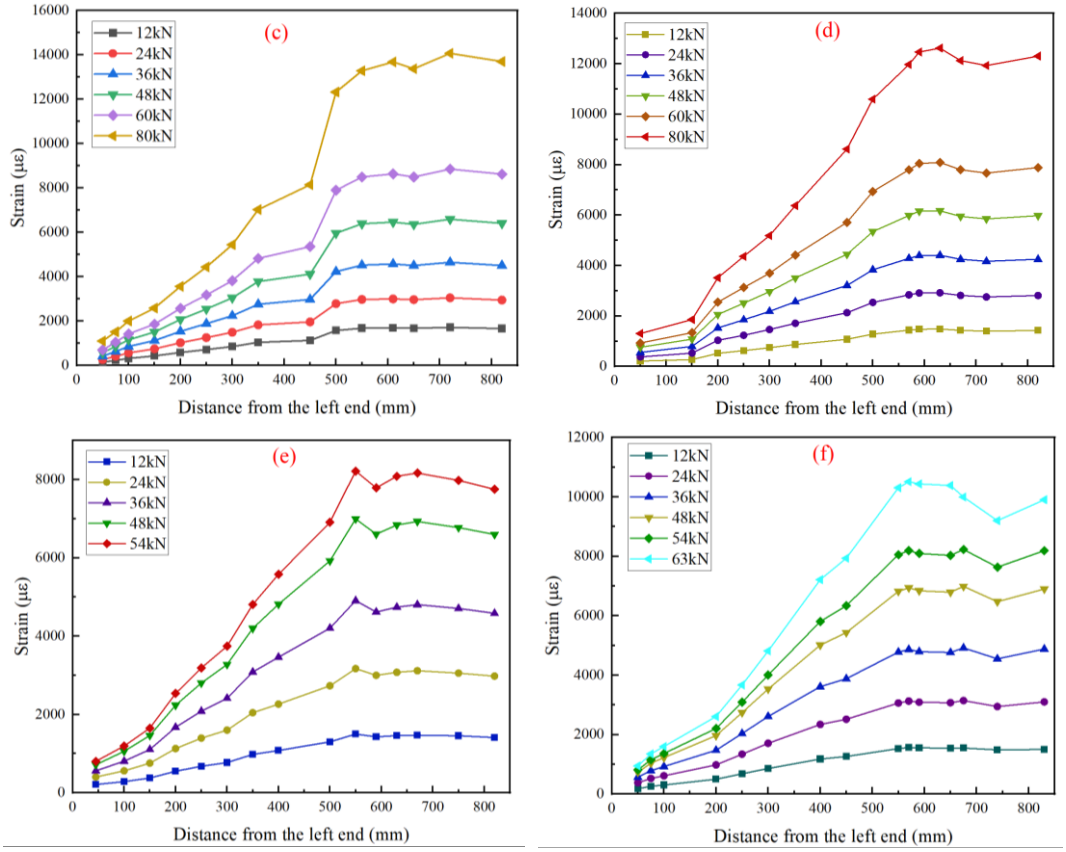

Fig. 9. Strain distribution at the bottom surface of some specimens: (a) CB1-A; (b) CB1-B; (c) CB3-A; (d) CB3-B; (e) GB1-A; and (f) GB1-B.

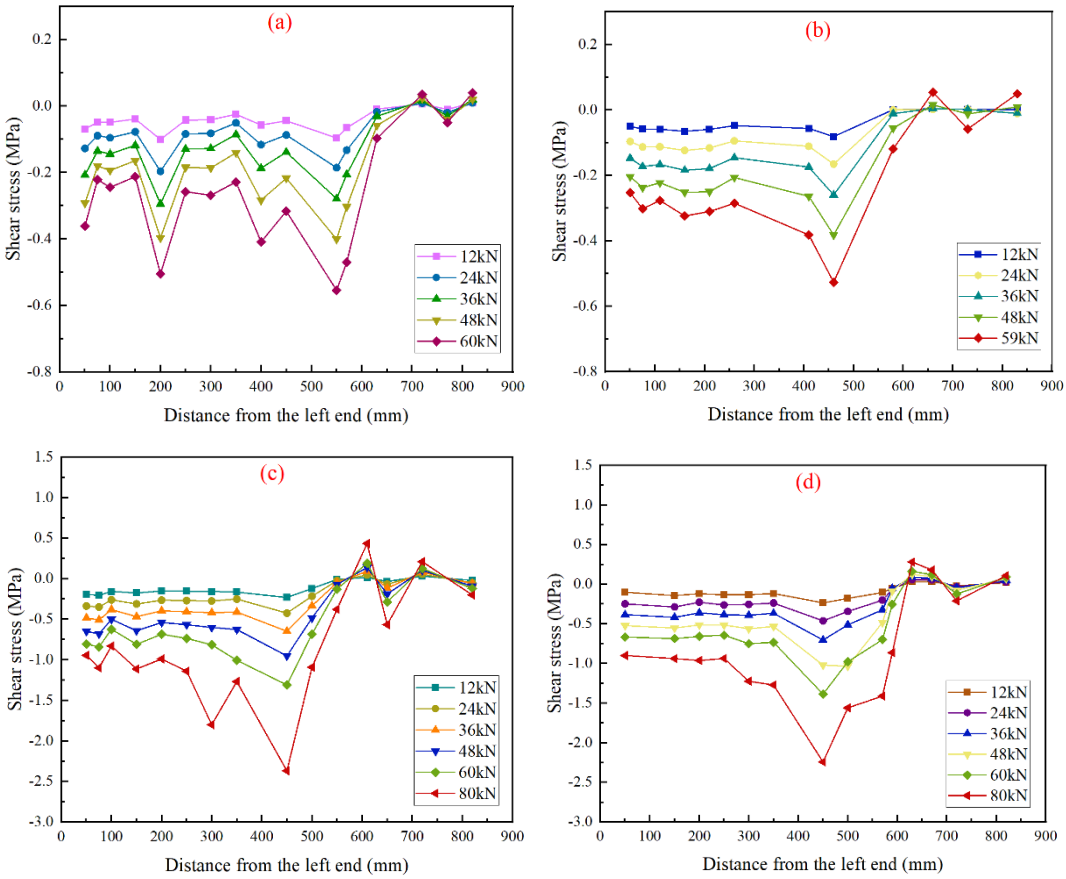

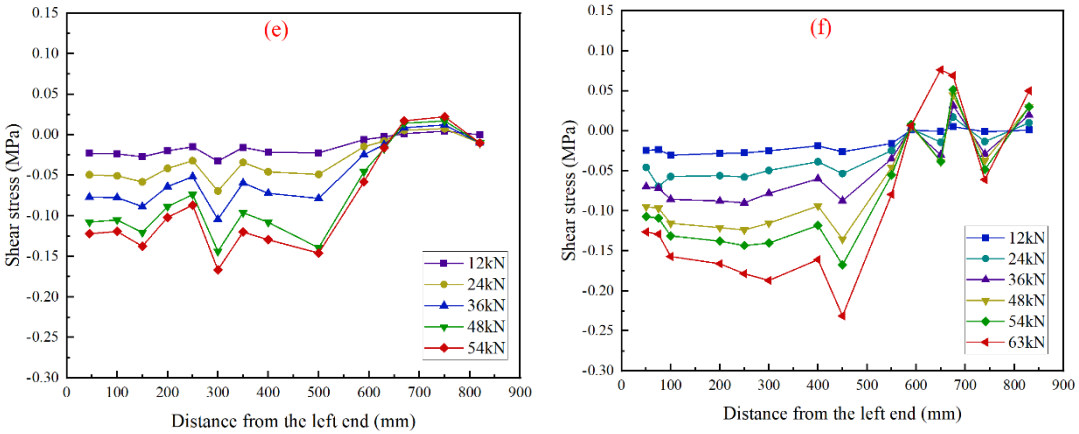

Fig. 10. Distribution of shear stress of the adhesive layer: (a) CB1-A; (b) CB1-B; (c) CB3-A; (d) CB3-B; (e) GB1-A; and (f) GB1-B.

Fig. 9 presents the strain distribution on the bottom surface of some of the specimens. At the same load level, the FRP strain increases approximately linearly along the longitudinal direction in the bending and shearing section of the specimen, while in the purely bending section, the strain is basically distributed in a horizontal fluctuation, which is attributed to an error in the actual position and orientation of the strain gauges. It can be found from **Fig. 9** that due to the local damage of the specimens, the purely bent sections of specimens GB1-B suffer a dramatic reduction in strain when subjected to bending near the ultimate load, resulting in a decrease of strain at the partially bamboo scrimber beam.

The measured strains in the FRP were converted into shear stresses of adhesive by taking Formula (5), as shown in **Fig. 10** (positive and negative represent direction only and are independent of the numerical magnitude). The shear section (50 mm-520 mm) can be seen, the shear stress of the adhesive layer increases accordingly with the rise in load and are approximately horizontally distributed, and the non-existence of high stress at the plate-end can be observed. In purely bending part (620 mm-850 mm), with an increasing load, interfacial shear stress always fluctuates in a horizontal sawtooth pattern above and below 0, which leads to higher fluctuation ranges of shear stress. The stress transition region (520 mm-620 mm) is near the loading point, and the shear stress of the adhesive layer gradually decreases to 0 in the transition region. When all specimens are subjected to the ultimate load, the maximum shear stress of the adhesive layer is basically located close to the loading point.

Given that the FRP thickness of specimens of Group 2 is thicker than that of group 1, the shear stress of the adhesive layer in the bending and shearing section of specimens CB3-A and CB3-B of Group 2 are greater than those of CB1-A and CB1-B of Group 1 under the same load. Similarly, compared to Group 3, as the modulus of elasticity of CFRP is higher than that of GFRP, and the interfacial shear stresses at the adhesive layer of specimens CB1-A and CB1-B in Group 1 are larger than those of GB1-A and GB1-B in Group 3.

4. Analytical model of adhesive layer shear stress

4.1 Theoretical calculation model

Considering the thin thickness of the adhesive layer of the specimen, the two-parameter model was hereby adopted to study the forces of the adhesive layer of FBSCB, and to derive closed solutions for the shear stresses of the adhesive layer interface of FBSCB under four-point bending loads according to the equilibrium differential equations and displacement coordination conditions. The assumptions for the theoretical calculation are the same as those proposed in Section 3.3.

Fig. 11 describes the FRP- bamboo scrimber beam under a four-point bending load, where it can be observed that the overall coordinate origin is located at the left end of the central axis of the adhesive layer, and the X axis is located at the central axis of the adhesive layer. In order to distinguish between the length and width of the bamboo scrimber beam, the FRP reinforcement and the adhesive layer were denoted as L and b, respectively. The symbols for bamboo scrimber beam were subscripted as 1, for

FRP as 2 and for glue layer as a; z_1, z_2 and h_a were used for the depth of bamboo, FRP and adhesive layer, respectively.

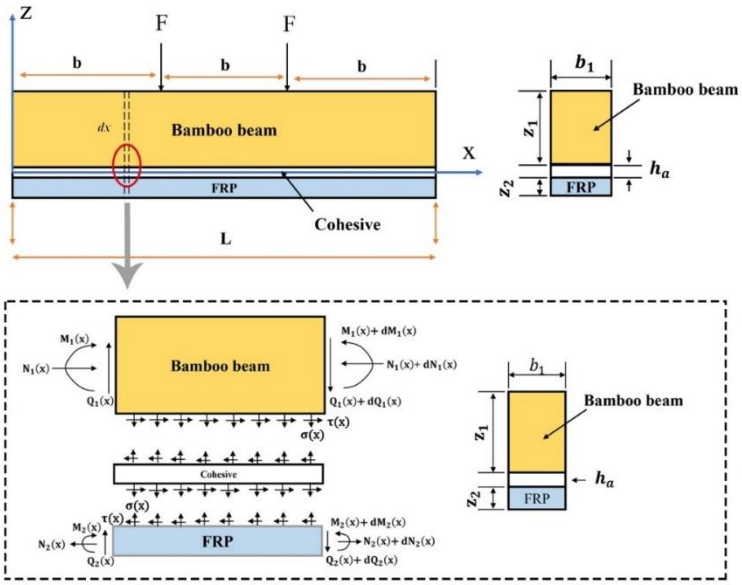

Fig. 11. FBSCB under four-point bending load and differential sections of FBSCB.

Take a differential section *dx* from the composite beam displayed in **Fig. 11**. The positive and shear stresses of the adhesive layer interface are $\sigma(x)$ and $\tau(x)$, and the equilibrium equations are established as follows.

$$\frac{dN_1(x)}{dx}=b_2\tau(x)\quad \frac{dN_2(x)}{dx}=b_2\tau(x) \tag{6}$$

$$\frac{dQ_1(x)}{dx}=-b_2\sigma(x)\quad \frac{dQ_1(x)}{dx}=-b_2\sigma(x) \tag{7}$$

$$\frac{dM_1(x)}{dx}=Q_1(x)-b_2\tau(x)\frac{z_1}{2}\quad \frac{dM_2(x)}{dx}=Q_2(x)-b_2\tau(x)\frac{z_2}{2} \tag{8}$$

where, $N_1(x)$ and $N_2(x)$, $Q_1(x)$ and $Q_2(x)$, $M_1(x)$ and $M_2(x)$ are the internal axial force, transverse shear force and bending moment in the cross section of the bamboo scrimber beam and FRP center axis, respectively.

The relationship between shear stress and shear strain can be written as:

$$\tau(x)=G\gamma_{xz} \tag{9}$$

where, G is the shear modulus and γ_{xz} is the shear strain as follows:

$$\gamma_{xz}=\frac{dv(x,y)}{dx}+\frac{du(x,y)}{dy} \tag{10}$$

where, $u(x,y)$, $v(x,y)$ represent the horizontal and vertical displacements of the composite beam at any position respectively. Substituting Eq. (10) into Eq. (9), differentiate once:

$$\frac{d\tau(x)}{dx}=G_a\left(\frac{d^2v(x,y)}{dx}+\frac{d^2u(x,y)}{dx}\right) \tag{11}$$

the adhesive layer is assumed to be subjected to a uniform shear stress, so that the horizontal displacement of the adhesive layer follows linearly along the adhesive layer thickness h_a, then:

$$\frac{du}{dy}=\frac{u_2(x)-u_1(x)}{h_a} \tag{12}$$

where, $u_1(x)$ and $u_2(x)$ are longitudinal displacements at the bottom of the reconstituted bamboo

beam and the top of the FRP, respectively, and then simultaneously differentiate both sides x of Eq. (12) above as follows:

$$\frac{d^2u(x,y)}{dydx}=\frac{1}{h_a}\left(\frac{du_2(x)}{dx}-\frac{du_1(x)}{dx}\right) \tag{13}$$

The relationship between the curvature of a bending beam and the bending moment is given by:

$$\frac{d^2v(x)}{dx^2}=-\frac{M_T(x)}{(EI)_t} \tag{14}$$

Taking Eq. (13) and Eq. (14) into Eq. (11) gives

$$\frac{d\tau(x)}{dx}=\frac{G_a}{h_a}\left(\frac{du_2(x)}{dx}-\frac{du_1(x)}{dx}-\frac{h_aM_T(x)}{(EI)_t}\right) \tag{15}$$

where, G_a is the modulus of elasticity of the adhesive layer, and $(EI)_t$ denotes the flexural stiffness of the composite beam. However, the third term in parentheses in the above equation is very small and is therefore ignored for the ease of subsequent calculations.

As shown in **Fig. 11** above, considering the deformation of the three components of axial, bending moment and shear deformation, the longitudinal displacements of the bamboo scrimber beam and FRP surface can be obtained as follows:

$$\begin{aligned}\varepsilon_1(x)&=\frac{du_1(x)}{dx}=-\frac{N_1(x)}{E_1A_1}-\frac{h_1}{\alpha G_1A_1}\left[-b_2\sigma(x)-F\right]+\frac{h_1}{E_1I_1}M_1(x)\\ \varepsilon_2(x)&=\frac{du_2(x)}{dx}=\frac{N_2(x)}{E_2A_2}+\frac{h_2}{\alpha G_2A_2}b_2\sigma(x)-\frac{h_2}{E_2I_2}M_2(x)\end{aligned} \tag{16}$$

Substituting Eq. (16) into Eq. (15) yields:

$$\frac{d\tau(x)}{dx}=\frac{G_a}{h_a}\left[\frac{N_2(x)}{E_2A_2}+\frac{h_1}{\alpha G_2A_2}b_2\sigma(x)-\frac{h_2}{E_2I_2}M_2(x)+\frac{N_1(x)}{E_1A_1}-\frac{h_1}{\alpha G_1A_1}\left[-b_2\sigma(x)-F\right]-\frac{h_1}{E_1I_1}M_1(x)\right] \tag{17}$$

where, E_1, E_2 are the modulus of elasticity of reconstituted bamboo and FRP respectively, α, the shear factor taken as $5/6$; h_1 and h_2, the distances from the top and bottom of the adhesive layer to the respective centroids of the beam and FRP; and A, the cross sectional area.

Assuming that the curvature of the bamboo scrimber beam and FRP sheet are the same, the relationship between $M_1(x)$ and $M_2(x)$ is:

$$M_1(x)=RM_2(x) \tag{18}$$

where

$$R=\frac{E_1I_1}{E_2I_2} \tag{19}$$

The equilibrium equation for the bending moment can be given in **Fig. 11** above as:

$$M_T(x)=M_1(x)+M_2(x)+N(x)(h_1+h_2+h_a) \tag{20}$$

The combination of Eq. (6) shows that

$$N_1(x)=N_2(x)=N(x)=b_2\int_0^x\tau(x)dx \tag{21}$$

From Eq. (19) to Eq. (22) $M_1(x)$ and $M_2(x)$ are given as:

$$\begin{aligned}M_1(x)&=\frac{R}{R+1}\left[M_T(x)-b_2\int_0^x\tau(x)(h_1+h_2+h_a)dx\right]\\ M_2(x)&=\frac{1}{R+1}\left[M_T(x)-b_2\int_0^x\tau(x)(h_1+h_2+h_a)dx\right]\end{aligned} \tag{22}$$

Differentiating $M_1(x)$ and $M_2(x)$ gives the shear stress forces $Q_1(x)$ and $Q_2(x)$:

$$Q_1(x)=\frac{dM_1(x)}{dx}=\frac{R}{R+1}\left[Q_T(x)-b_2\tau(x)(h_1+h_2+h_a)\right]$$
$$Q_2(x)=\frac{dM_2(x)}{dx}=\frac{1}{R+1}\left[Q_T(x)-b_2\tau(x)(h_1+h_2+h_a)\right] \tag{23}$$

Differentiate Eq. (17) once and then substitute it into Eq. (6) and Eq. (23):

$$\frac{d^2\tau(x)}{dx^2}-\frac{G_ab_2}{h_a}\left(\frac{1}{E_1A_1}+\frac{1}{E_2A_2}+\frac{(h_1+h_2)(h_1+h_2+h_a)}{E_1I_1+E_2I_2}\right)\tau(x)+\frac{G_a}{h_a}\left(\frac{h_1+h_2}{E_1I_1+E_2I_2}\right)Q_T(x)$$
$$+\frac{G_ab_2}{h_a}\left(\frac{h_1}{\alpha G_1A_1}-\frac{h_2}{\alpha G_2A_2}\right)\frac{d\sigma(x)}{dx}=0 \tag{24}$$

To obtain a simple closed solution, referring to Smith's [17] solving approach, the effect of shear deformation is neglected. When the loading is in four-point bending $d^2Q_T(x)/dx^2=0$, then:

$$\frac{d^2\tau(x)}{dx^2}-\frac{G_ab_2}{h_a}\left(\frac{1}{E_1A_1}+\frac{1}{E_2A_2}+\frac{(h_1+h_2)(h_1+h_2+h_a)}{E_1I_1+E_2I_2}\right)\tau(x)+\frac{G_a}{h_a}\left(\frac{h_1+h_2}{E_1I_1+E_2I_2}\right)Q_T(x)=0 \tag{25}$$

The general solution $\tau(x)$ for the shear stress in the adhesive layer can be found as:

$$\tau(x)=B_1\cosh(\lambda x)+B_2\sinh(\lambda x)+m_1Q_T(x) \tag{26}$$

where,

$$\lambda^2=\frac{G_ab_2}{h_a}\left(\frac{1}{E_1A_1}+\frac{1}{E_2A_2}+\frac{(h_1+h_2)(h_1+h_2+h_a)}{E_1I_1+E_2I_2}\right)$$
$$m_1=\frac{G_a}{h_a\lambda^2}\left(\frac{h_1+h_2}{E_1I_1+E_2I_2}\right) \tag{27}$$

When the composite beam is subjected to a four-point bending stress, the shear stress in the adhesive layer is divided into two parts:

$$\tau(x)=\begin{cases}B_1\cosh(\lambda x)+B_2\sinh(\lambda x)+m_1F, & 0\le x\le b\\ B_3\cosh(\lambda x)+B_4\sinh(\lambda x), & b\le x\le \dfrac{L}{2}\end{cases} \tag{28}$$

where, the unknown parameters B_1, B_2, B_3 and B_4 can be determined by the following boundary conditions:

at $x=0$, $M_1(0)=M_T(0)=0$; at $x=\frac{L}{2}$, $\tau\left(\frac{L}{2}\right)=0$; at $x=b$, $\tau_1(x)\big|_{x=b}=\tau_2(x)\big|_{x=b}$; at $x=b$,

$$\frac{d\tau_1(x)}{dx}\Big|_{x=b}=\frac{d\tau_2(x)}{dx}\Big|_{x=b} \tag{29}$$

The first boundary condition is that the axial force $N_1(x)=N_2(x)=0$ and the corresponding bending moment $M_1(0)=M_2(0)=0$ for the FRP and the reconstructed bamboo beam at x = 0. The second boundary condition should be zero for the interface shear stress in the span due to the forces symmetrical along the neutral axis to which the composite beam is subjected. The third and fourth boundary conditions are to ensure the continuity of the shear stresses and their first derivatives under symmetric loading.

The constants are consequently determined to be:

$$B_1=-m_1Fe^{-k},\quad B_2=0,\quad B_3=0,\quad B_4=-m_1F\sinh(k) \tag{30}$$

Substituting these expressions into Equation (28) gives

$$\tau(x)=\begin{cases}-m_1F\cosh(\lambda x)e^{-k}+m_1F, & 0\le x\le b\\ m_1F\sinh(k)e^{-\lambda x}, & b\le x\le \dfrac{L}{2}\end{cases} \tag{31}$$

4.2 Finite element model

FBSCB are multi-layered composite structures, consisting of FRP, adhesive layer and bamboo scrimber. Thus, it is necessary to build a finite element model of the composite beam to reveal in detail the distribution of stress of the adhesive layer under a four-point bending load.

Fig. 12(a) presents a FEM built with the CB1-A specimen. In the case of building the FEM, by using Cohesive zone model (CZM), establishing a traction-separation criterion, selecting a quadratic nominal stress criterion (Quads Damage) and B-K criterion, and assigning the Cohesive property to the adhesive layer interface, the adhesive layer was simulated, as the adhesive layer was very thin (usually less than 1mm). The bamboo scrimber beams and the FRP laminates were modeled using four-node reduced integration quadrilateral shell element (S4R), and the FRP nodes correspond to the bamboo scrimber beams nodes. The adhesive layer was modeled using eight-node cohesive element (COH3D8), with nodes shared with FRP and the bamboo scrimber beams, respectively. Their material properties were described above. For bamboo scrimber beam, when four-point bending was performed, plastic material was applied at the upper part under compression, and elastic material was applied at the lower part under tension, according to the central axis along the height direction. FRP layer was assumed to be an elastic material. To improve the accuracy of the results, the mesh was partially refined, as shown in **Fig. 12**(b) below. The bottom of the bamboo scriber beam was refined with a mesh size in keeping with the adhesives layer, measuring 0.36 mm. For the rest, the mesh size was 2 mm to improve efficiency. The X, Y and Z movement DOFs were constrained at the left support node, while the Y and Z movement DOFs were constrained at the right support. A symmetrical concentrated load P was applied at the three points of the composite beam.

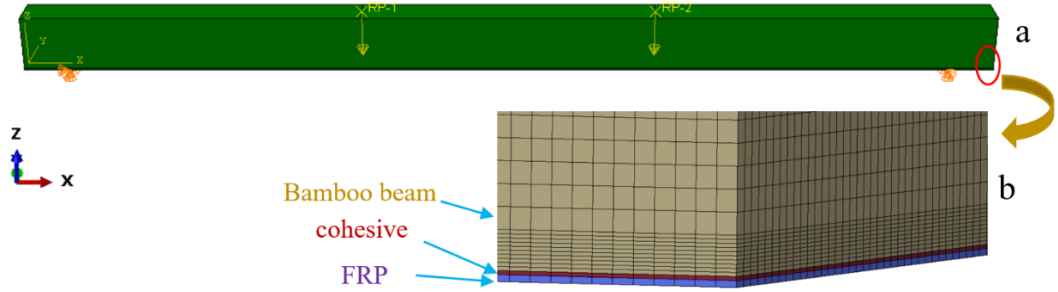

Fig. 12. (a) Finite element model of specimen CB1-A; (b) Partial refinement of the mesh.

4.3 Model validation

Fig. 13 shows the comparison of shear stress of the adhesive layer obtained from the test results, theoretical calculations and finite element simulations. **Fig. 13**(a) and (b) present the shear stress of the adhesive layer of specimen CB1-B at 36 kN and 48 kN, **Fig. 13**(b) and (c) depict the shear stress of the adhesive layer of the CFRP and GFRP composite beam at 48 kN, and **Fig. 13**(b) and (d) illustrate the shear stress of the adhesive layer of the one-layer CFRP and three-layer CFRP composite beam at 48 kN.

Table 5. Average shear stress of the adhesive layer at the bending and shearing zone

Model	CB1-B 36kN (MPa)	CB1-B 48 kN (MPa)	GB1-B 48 kN (MPa)	CB3-B 48 kN (MPa)
Test results	0.18	0.24	0.10	0.53
FEM	0.23	0.30	0.11	0.78
Theoretical calculations	0.19	0.25	0.09	0.67

It can be seen from the **Fig. 13** that the trend in the distribution of shear stress of the adhesive layer is approximately the same for all four specimens, but there are differences in detail. For shear stress of

the adhesive layer in the bending and shearing zone (50-520 mm) at each measurement point, the theoretical calculated values are exactly equal, the finite element simulation values show three stages of increasing, remaining approximately equal and slightly increasing, and the test results fluctuate horizontally. Both finite element model and experimentally measured shear stress of the adhesive layer are observed at a peak stress around 500 mm. During the transition zone (520-620 mm), shear stress of the adhesive layer nearly decreases in a stepwise manner, with a short distance in the falling stage, while the simulated FEM and test results show a gradual decline with a long distance through the falling stage. For shear stress of the adhesive layer in the pure bending zone (620-850 mm) at all measurement points, the theoretically calculated values are identical, the finite element simulated values show slight fluctuations, and the experimentally measured values exhibit a wider range of fluctuations.

Table 5 presents the average shear stress of the adhesive layer in the bending and shearing zone. The average shear stress of the adhesive layer between the finite element simulations and the theoretical calculations for the four groups of specimens are in error and are 17.4%, 16.7%, 18.2% and 14.1%, respectively, which is caused by assuming the bamboo scrimber beam and FRP as Euler-Bernoulli beams in the theoretical calculations while ignoring their shear deformation. The average shear stress of the adhesive layer errors between the finite element simulation and test results for the four groups of specimens are 27.8%, 25.0%, 10.0% and 47.2%, respectively, while the errors between the theoretical calculations and test results are 5.5%, 4.1%, 10.0% and 26.4%, respectively. This reveals that both the finite element simulation and the theoretical calculation errors tend to remain stable when only the load changes, such as specimen CB1 at loads of 36 kN and 48 kN. However, given that shear stress of the adhesive layer of test results is averaged from the strains on the FRP surface, which leads to increased test errors with rising FRP thickness, the error will increase with increasing thickness when the number of FRP layers increases, as in specimen CB1-B and specimen CB3-B.

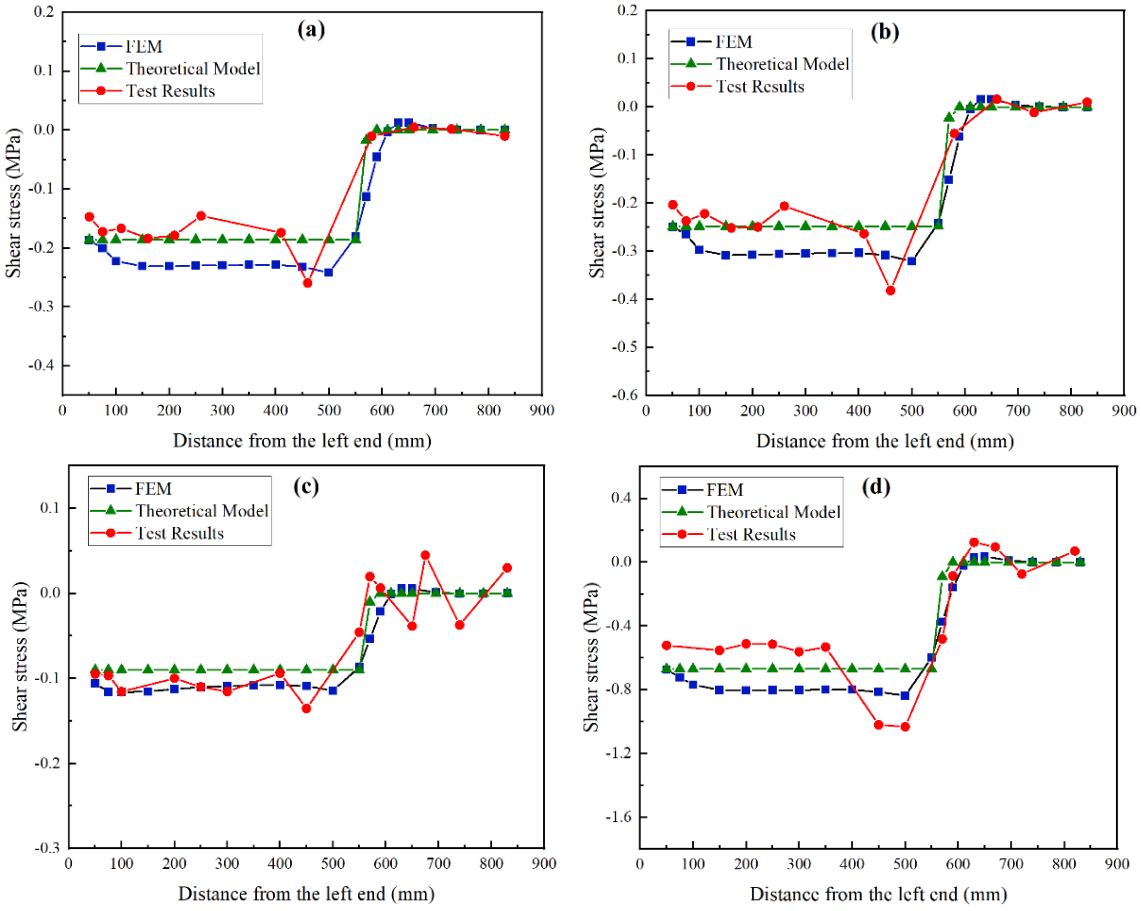

Fig. 13. Comparison of test results, theoretical calculations and finite element simulation for three models of shear stress of the adhesive layer: (a) and (b) CB1-B at 36 kN and 48 kN; (c) GB1-B at 48 kN; and (d) CB3-B at 48 kN.

In conclusion, the theoretical calculated solution for shear stress of the adhesive layer fluctuates little, but the shear deformation of the bamboo scrimber beam and FRP is ignored, and the detailed changes at the ends of the bending and shearing zone as well as the transition zone cannot be reflected. The test results overall indicate the change in interfacial shear stress of the adhesive layer, but the fluctuation ranges widely and the test error increases with increasing FRP thickness. The FEM uses CZM to simulate the cohesive layer, which not only shows the detailed variation of the shear stress of the adhesive layer, but also has a less fluctuation range. Besides, it can better analyze the interfacial shear stress of the adhesive layer.

4.4 Parametric study

The effect of FRP types and thickness on the interfacial stress at the adhesive layer was hereby investigated based on a comparison of three types of results including the test results, theoretical calculation and finite element simulation.

4.4.1 Effect of FRP types

Fig. 14(a) shows the effect of different FRP types on the shear stress at the interface of the composite beam adhesive layer, which was modelled as GB1-B and CB1-B in this study. The overall distribution of shear stress of the adhesive layer for the different FRP types follows the same trend in the three results. In the bending and shearing zone, the average shear stress of the adhesive layer for the GFRP composite beam and CFRP composite beam in the three results are 0.01 MPa and 0.24 MPa, 0.09 MPa and 0.25 MPa, 0.11 MPa and 0.38 MPa, respectively. The modulus of elasticity of GFRP and CFRP is 31.2 GPa and 90.1 GPa, respectively, while that of elasticity of CFRP is nearly three times that of GFRP. When the modulus of elasticity is increased 3 times, the bond shear stress increases 2.62 times on average for all three results, indicating that the average shear stress of the adhesive layer is approximately linearly related to the FRP modulus of elasticity, which increases with the rise of the modulus of elasticity. In the pure bending zone, the shear stress of adhesive layer for all three results remains around the value of 0.

4.4.2 Effect of FRP thickness

The effect of FRP thickness on the tangential stresses at the bonding interface of the composite beam is represented in **Fig. 14**(b), modelled as CB1-B and CB3-B. The overall distribution of shear stress of the adhesive layer is the same for all three results when the FRP is 1 or 3 layers. For the bending and shearing zone, the shear stress of adhesive layer in the three results are 0.24 MPa and 0.53 MPa, 0.25 MPa and 0.67 MPa, 0.3 MPa and 0.8 MPa, respectively. It can be observed that the shear stress of the adhesive layer interface grows with the thickness of the FRP sheet, which increases 2.51 times on average when the FRP thickness increases 3 times. The shear stress of the adhesive layer is approximately linearly related to the FRP thickness. Besides, in the pure bending section, the shear stress of the adhesive layer remains around the value of 0 for all three FRP thicknesses.

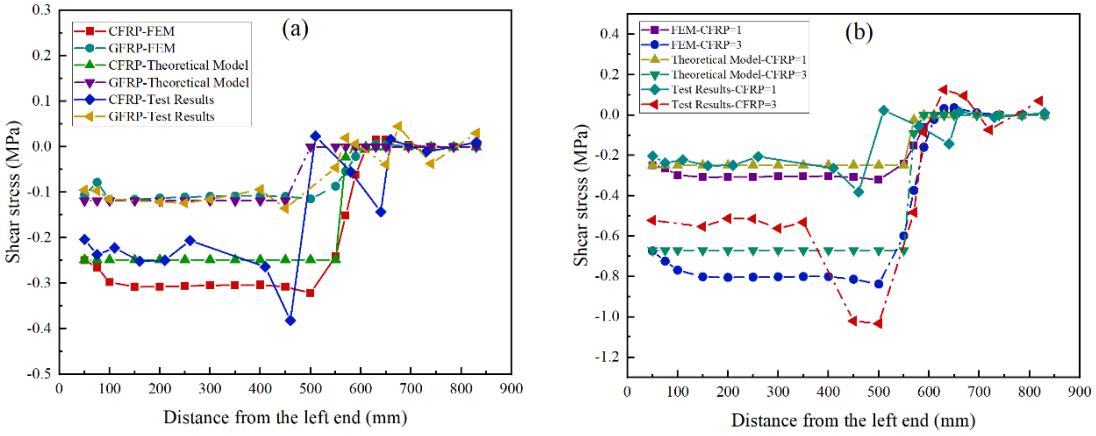

Fig 14. Effect of different parameters on the shear stress of the adhesive layer at 48kN: (a) effect of FRP types; and (b) effect of FRP thickness.

5. Conclusions

The four-point bending test method, finite element simulation and two-parameter model theoretical calculation were hereby adopted to research the stress distribution of the adhesive layer of FRP- bamboo scrimber composite beams, and the following conclusions can be drawn:

(1) The validity of the FEM of CZM and the two-parameter theoretical calculation model is verified through the four-point bending experimental data;

(2) FEM of the shear stress at the adhesive layer interface not only reflects the detailed changes, but also fluctuates smally, which can provide a better analysis of the shear stress at the adhesive layer. Besides, the two-parameter theoretical solution ignores the shear deformation of the bamboo scrimber beam and FRP, failing to describe the detailed changes of shear stresses at the two ends of the bending and shearing zone as well as the transition zone;

(3) There are three zones of shear stress at the adhesive layer of FBSCB under four-point bending load, i.e., the bending and shearing zone (50-520mm), the transition zone (520-620mm) and the pure bending zone (620-850mm). The shear stress of the adhesive layer is horizontally distributed in the bending and shearing zone, decreases rapidly to 0 in the transition section, and is almost 0 in the pure bending section;

(4) The influence of FRP type and FRP thickness on the stress of the adhesive layer is investigated. In the bending and shearing zone, the stress of the adhesive layer increase 2.51 times and 2.6 times when the thickness and elastic modulus of the FRP in the composite beam increase 3 times. The yield and ultimate loads of the composite beam with 3 layers of CFRP are greater than those with 1 layer, and its yield and ultimate displacements are also greater than those of the composite beam with 1 layer of CFRP;

(5) The result of this study can be applied to any reinforced composite beam containing adhesive layers to obtain the distribution of shear stresses at the adhesive layer interface in a four-point bending state.

Disclosure statement

The authors declare that they have no conflicts of interest to report regarding the present study

Funding Statement

The project is supported by Natural Science Foundation of Hunan Province (No 2020JJ5986), Hunan Provincial Department of Education Project (No 19B591), China Postdoctoral Science Foundation (No 2021M690768) and The science and technology innovation program of Hunan Province（No 2020RC4049）.

References

[1] Huang Z, Sun Y. Hygrothermal performance comparison study on bamboo and timber construction in Asia-Pacific bamboo areas. Construction and Building Materials 2020. https://doi.org/10.1016/j.conbuIldmat.2020.121602.

[2] Koh CH, Kraniotis D. Hygrothermal performance, energy use and embodied emissions in straw bale buildings. Energy & Buildings, 2021, 245. https://doi.org/10.1016/j.enbuild.2021.111091.

[3] Fan ZT, Wu JZ, Ma C. Analysis on the factors influencing Chinese bamboo and rattan product export under the background of global supply chain. Forest Engineering 2021; 37(5): 127-136. https://doi.org/10.16270/j.cnki.slgc.2021.05.002

[4] Huang Y, Ji Y, Yu W. Development of bamboo scrimber: A literature review. Journal of Wood Science 2019; 65(1): 1-10. https://doi.org/10.1186/s10086-019-1806-4

[5] Zheng, J, Shu, BQ, Xiao, ZP, Zhong, P. Advantages and disadvantages of new building material recombinant bamboo's development. Wood Processing Machinery 2017; 28(1), 39-42.

[6] Wang X, Luo X, Ren H, et al. Bending failure mechanism of bamboo scrimber. Construction and Building Materials 2022; 326: 126892. https://doi.org/10.1016/j.conbuildmat.2022.126892

[7] Wu XZ, Huang X, Li XJ, et al. Flexural performance of CFRP-bamboo scrimber composite beams. Journal of Renewable Materials 2019; 7(12): 1295-1307. https://doi.org/10.32604/jrm.2019.07839

[8] Wei Y, Ji X, Duan M, et al. Flexural performance of bamboo scrimber beams strengthened with f

iber-reinforced polymer. Construction and Building Materials 2017; 142: 66-82. https://doi.org/10.1016/j.conbuildmat.2017.03.054

[9] Chen S, Wei Y, Peng D, et al. Experimental investigation of timber beams strengthened by bamboo scrimber with anchorage structure. Structures 2021; 33: 1-11. https://doi.org/10.1016/j.istruc.2021.04.038

[10] Wei Y, Yan S, Zhao K, et al. Experimental and theoretical investigation of steel-reinforced bamboo scrimber beams. Engineering Structures 2020; 223: 111179. https://doi.org/10.1016/j.engstruct.2020.111179

[11] Donadon BF, Mascia NT, Vilela R, Trautwein LM. Experimental investigation of glued-laminated timber beams with Vectran-FRP reinforcement. Engineering Structures 2020; 202: 109818. https://doi.org/10.1016/j.engstruct.2019.109818

[12] Imjai T, Setkit M, Figueiredo FP, et al. Experimental and numerical investigation on low-strength RC beams strengthened with side or bottom near surface mounted FRP rods. Structure and Infrastructure Engineering 2022; 1-16. https://doi.org/10.1080/15732479.2022.2045613

[13] Pan B, Liu F, Zhuge Y, et al. ECCs/UHPFRCCs with and without FRP reinforcement for structural strengthening/repairing: A state-of-the-art review. Construction and Building Materials 2022; 316: 125824. https://doi.org/10.1016/j.conbuildmat.2021.125824

[14] Sanginabadi K, Yazdani A, Mostofinejad D, et al. RC members externally strengthened with FRP composites by grooving methods including EBROG and EBRIG: A state-of-the-art review. Construction and Building Materials 2022; 324: 126662. https://doi.org/10.1016/j.conbuildmat.2022.126662

[15] Wei Y, Yan SC, CHEN S, LB, et al. Numerical simulation on bending performance of FRP reinforced bamboo beams. Acta Materiae Compositae Sinica 2019; 36(4): 1036-1044.

[16] Goland M, Reissner E. The stresses in cemented joints. Journal of Applied Mechanics 1944; 11: A17-27.

[17] Smith ST, Teng JG. Interfacial stresses in plated beams. Engineering Structures 2001. https://doi.org/10.1016/S0141-0296(00)00090-0

[18] Wang J, Zhang C. Three-parameter elastic foundation model for analysis of adhesively bonded joints. International Journal of Adhesion and Adhesives 2009; 29:495-502. https://doi.org/10.1016/j.ijadhadh.2008.10.002

[19] Chen F, Qiao P. On the intralaminar and interlaminar stress analysis of adhesive joints in plated beams. International Journal of Adhesion and Adhesives 2012; 36:44-55. https://doi.org/10.1016/j.ijadhadh.2012.03.005

[20] Du Y, Liu Y, Zhou F. An improved four-parameter model on stress analysis of adhesive layer in plated beam. International Journal of Adhesion and Adhesives 2019; 91: 1-11. https://doi.org/10.1016/j.ijadhadh.2019.02.005

[21] Wu X Z, Yang W K, Li X J. Study on stripping mechanism of steel plate strengthened with carbon fiber reinforced polymer by cohesive zone model. Advances in Structural Engineering, 2020; 23(12): 2503-2513. https://doi.org/10.1177/1369433220912348

[22] ASTM D143-09: standard test methods for small clear specimens of timber, 2000.

[23] ASTM D 695-02a: standard test method for compressive properties of rigid plastics, American Society for Testing and Materials, 2002.

[24] GB/T 3354-1999: Test method for tensile properties of oriented fiber reinforced plastics, Standards Press of China, 1999. (in Chinese).

[25] ASTM D 198-09: standard test methods for static tests of lumber in structural sizes, American Society for Testing and Materials, 2009.

[26] Zhen HG, Xu DS. Reinforced concrete theory and analyse. Beijing, China: Tsinghua University Press Limited, 2003. (in Chinese).